Finite Element Modeling of Non-equilibrium Fluid-Wall Interaction at High-Mach Regime

Marie-Eve Dumas[1], Wagdi G. Habashi[2]

CFD Laboratory McGill University, Montreal, Quebec, H3A 2S6, Canada

Guido S. Baruzzi[3] and Dario Isola[4]

ANSYS Canada, Montreal, QC, H3A 2M7, Canada

Marco Fossati[5]

Aerospace Center of Excellence, University of Strathclyde, Glasgow, G1 5HE, UK

The numerical modeling of the aerodynamic interactions at high-altitudes and high-Mach numbers is considered in view of its importance when studying problems where the continuum hypothesis at the foundation of the Navier-Stokes equations becomes invalid. One of the difficulties associated with these flight conditions is that both the velocity and the temperature of the fluid do not abide by the no-slip conditions at the wall. A weak-Galerkin Finite Element formulation of the Maxwell-Smoluchowsky model is introduced to discretize the velocity slip and temperature jump conditions with better accuracy than the standard Finite Element approximation. The methodology is assessed on configurations such as cylinders and spheres for flow conditions ranging from quasi-equilibrium to non-equilibrium. Improvements are observed in the slip regime compared to available data. Nonetheless, the results in the transition regime highlight the need for more sophisticated physical modeling to address non-equilibrium at the wall.

---

[1] Graduate student, Department of Mechanical Engineering, 688 Sherbrooke Street West.

[2] Professor and Director CFD Laboratory, Department of Mechanical Engineering, 688 Sherbrooke Street West, AIAA Fellow.

[3] R&D Director, ANSYS Canada, 680 Sherbrooke Street West, AIAA Member.

[4] R&D, ANSYS Canada, 680 Sherbrooke Street West, AIAA Member.

[5] Lecturer, Department of Mechanical and Aerospace Engineering, 75 Montrose Street, AIAA Member.

I. Introduction

THE numerical study of high-Mach, high-altitude flows requires the modeling of non-equilibrium conditions dictated by the small residence times of fluid dynamics and the reduced molecular collision frequencies. Accurate numerical simulation of such flows is essential, given the fundamental role of CFD in the design of future high-speed aircraft and the high costs and known limits of hypersonic wind tunnels [1]. A critical phenomenon that needs to be addressed is the breakdown of the local equilibrium assumption. The validity of the Navier-Stokes equations (N-S) is based on the hypothesis that the gas is in quasi-local thermodynamic equilibrium, which is true when the frequency of molecular collisions is sufficiently high compared to the typical residence time of a fluid particle. At high altitude, or when rarefaction effects occur, the density, and therefore the number of molecules per unit volume is low and thus the collision frequency is reduced. A similar non-equilibrium condition is observed in regions where large gradients of bulk quantities coexist with small residence times caused by very high speeds. In both cases, departure from equilibrium is significant, and when interacting with aircraft surfaces, the fluid slips (velocity slip) over the surface and the temperature of the fluid in contact with the wall does not match the temperature of the body (temperature jump) [2].

The degree of non-equilibrium is measured by the Knudsen number (Kn), defined as the ratio between the mean-free-path of the molecules of the gas and a suitable characteristic length [3, 4]. Four different flow regimes can be identified according to the Knudsen number. For $Kn < 0.01$, the continuum hypothesis holds true and the flow can be appropriately described by the Navier-Stokes equations (N-S). For Kn between 0.01 and 0.1, the so-called slip regime, non-equilibrium effects become more relevant, especially in the proximity of the walls. The fluid can still be analyzed using the N-S equations, but more complex wall boundary conditions are needed to account for the non-equilibrium effects. For Knudsen numbers between 0.1 and 10, the flow in said to be in the transitional regime, where the thermodynamic assumption of the N-S equations begins to break down and non-equilibrium effects become predominant. Finally, for $Kn > 10$, the flow is considered to be in the free-molecular regime, where simulation by particle-based techniques is required.

While particle-based methods, such as Direct Simulation Monte Carlo (DSMC), can be applied efficiently only to free-molecular regimes due to the limited number of particles to follow, hybrid methodologies that use N-S in regions of near-equilibrium / transitional regime, and particle-based methods in regions of rarefied flow [5-10] have

been published in the literature. Such strategies, however, are subject to inaccuracies caused by the exchange of information at the interface between the various regions and also due to the fact that DSMC is typically subject to statistical scatter that may negatively affect the continuum-based solution [5-10]. As a stratagem to delay the adoption of expensive particle-based methods, traditional continuum-based CFD codes can be modified to simulate flows in the moderate non-equilibrium region ($0.01 < Kn < 1$) by introducing boundary conditions that account for velocity slip and temperature jump at the wall. Several formulations of the slip and jump conditions derived from the kinetic theory of gases have been proposed following the seminal work of Maxwell [11, 12]. A common subclass of the Maxwell model is built for the special case of a flat plate, neglecting the gradient of velocity normal to the wall [13, 14]. Consequently, they are not easily applicable to geometries with strong curvature or for rotational motion [15-17]. Following the original work of Maxwell and subsequent developments from Lockerby and al., physical models for the fluid-wall interaction have been proposed incorporating the full form of the tangential shear stress, which naturally contains a term for the variation of the velocity normal to the body in the tangential direction. Such models are necessary to accurately simulate near-wall aerothermodynamics phenomena when addressing the slip and early transitional regimes in conjunction with continuum N-S models

Numerical inaccuracies arise when considering the approximation of the differential operators appearing in the temperature jump and velocity slip formulations. In the context of Finite Element Methods (FEM), the discretization of gradients is generally first-order accurate when capturing shocks. Such level of accuracy is inadequate for accurate predictions of wall shear stresses and heat fluxes needed in slip and jump models. An FEM discretization, referred to as the "Consistent-Galerkin Finite Element Method (abbreviated here as CGFEM)", is proposed to provide second order accurate spatial approximation of the differential operators [18, 19]. For high-speed non-equilibrium flows, CGFEM can provide the accuracy required to address the challenges of hypersonic aerothermodynamics design.

In Section II, the formulation of Maxwell's boundary condition for the velocity slip and Smoluchowski's formulation for the temperature jump are presented. Section III describes the numerical implementation of these models. Section IV presents examples of flows in the regime $0.01< Kn < 1$. Finally, in Section V, a systematic grid refinement analysis is performed to verify the order of accuracy of the proposed methodology.

II. Non-equilibrium Boundary Conditions

Several models have been proposed in the literature for the computation of the slip wall conditions, such as the Langmuir and wall-function slip models [1, 9, 12, 20-24]. Among these, the Maxwell and Smoluchowski approaches capture the physics over a wide range of flow conditions and geometries. Additionally, they can be extended to second order slip conditions by including second order derivatives of velocity and temperature for flows at higher Knudsen numbers.

A. Slip Velocity

In the original formulation of Maxwell [11], the velocity tangential to the wall is expressed in terms of the tangential components of shear stress and heat flux, $\boldsymbol{\tau}_{slip}$ and $\boldsymbol{q}_{slip}$. The wall velocity slip is thus

$$\mathbf{V}_{slip} = -\frac{\lambda}{\mu}\frac{2-\sigma_V}{\sigma_V}\boldsymbol{\tau}_{slip} - \frac{3}{4}\frac{(\gamma-1)\mathrm{Pr}}{\gamma P}\mathbf{q}_{slip} \tag{1}$$

where σ_V is the Tangential Momentum Accommodation Coefficient (TMAC), μ is the dynamic viscosity at the wall, λ is the molecular mean-free-path at the wall, Pr is the Prandtl number, γ is the specific heat ratio and P is the gas pressure. The mean-free-path is defined as:

$$\lambda = \frac{\mu}{\rho}\sqrt{\frac{\pi}{2RT}} \tag{2}$$

where ρ is the density, T is the temperature and R is the gas constant.

The accommodation coefficient σ_V represents the fraction of the gas molecules that are reflected diffusely when colliding with the wall. A TMAC of 0 represents an infinitely smooth surface, while a TMAC equals to 1 represents a rough wall with only diffuse interactions (fully diffuse wall). Experiments indicate that the TMAC ranges between 0.2 and 0.8 [25] and varies with the molecular weight of the gas, the surface material, the temperature and roughness of the surface. More recently, Sharipov and Saleznev [26] developed an expression for the velocity slip derived from kinetic analysis on curved surfaces [27]. By neglecting the thermal creep, the Maxwell velocity slip is re-written as

$$\mathbf{V}_{slip} = -\frac{\lambda}{\mu}A_\sigma\boldsymbol{\tau}_{slip}$$

where A_σ is a coefficient defined as

$$A_\sigma = \frac{2}{\sqrt{\pi}}\sigma_P \tag{3}$$

and, for planar flow, the slip coefficient, σ_P, can be written as

$$\sigma_P(\sigma_V) = \left(\frac{2-\sigma_V}{\sigma_V}\right)\left[\sigma_P(1) - 0.1211(1-\sigma_V)\right]$$

Albertoni et al. [28] derived a value for $\sigma_P(1)$ of 1.016191 from the Bhatnagar–Gross–Krook (BGK) model of the Boltzmann equation, which is commonly referred to as the most accurate value for $\sigma_P(1)$ in fully diffuse conditions. It will be used in this work to match the fully diffuse wall used in the simulations of the reference data [1, 29]. A TMAC of one will be used throughout this study as well to remain consistent with the available data. Using these values in (3), A_σ equates to 1.14665 in this case.

Equation (1) can be expressed in terms of wall shear stress, $\boldsymbol{\tau}_w$, and temperature gradient, ∇T_w, as:

$$\mathbf{V}_{slip} = -A_\sigma \frac{\lambda}{\mu}(\mathbf{n}\cdot\boldsymbol{\tau}_w)(\mathbf{I}-\mathbf{nn}) - \frac{3}{4}\frac{(\gamma-1)\mathrm{Pr}}{\gamma P}(k\nabla T_w - (k\nabla T_w\cdot\mathbf{n})\mathbf{n}) \tag{4}$$

n being the unit-vector normal to the wall and k being the thermal conductivity. In equation (4) the vector-tensor dot product is defined as

$$(\mathbf{n}\cdot\boldsymbol{\tau})^\alpha = \sum_{\beta=1}^{3} \mathrm{n}^\beta \boldsymbol{\tau}^{\beta\alpha} \qquad \text{and} \qquad (\boldsymbol{\tau}\mathbf{n})^\alpha = \sum_{\beta=1}^{3} \boldsymbol{\tau}^{\alpha\beta}\mathrm{n}^\beta \tag{5}$$

The vector-vector outer product is also introduced here as $\boldsymbol{c=ab}$, such that $c^{\alpha\beta} = a^\alpha b^\beta$. The Cartesian components of a vector/tensor being indicated with a superscript Greek letter, to distinguish them from the vertex index, i.e. a subscript Latin letter.

B. Temperature Jump

The Smoluchowski's formulation for the temperature jump [30] is

$$T_{slip} - T_{body} = \left(\frac{2-\sigma_T}{\sigma_T}\right)\frac{2\gamma}{(\gamma+1)\mathrm{Pr}}\lambda\nabla T\cdot\mathbf{n} \tag{6}$$

where σ_T is the temperature accommodation coefficient and T_{body} is the temperature at the wall. The accommodation coefficient σ_T is defined as the fraction of energy exchanged between the gas molecules and the surface. The value of the accommodation coefficient depends heavily on the surface and gas types. Studies show that it generally ranges between 0.3 - 0.9 [31]. A coefficient of unity (σ_T = 1) will be used in this work for compatibility with the DSMC model used in the reference data.

III. Finite Element Formulation

The velocity slip and temperature jump equations (4) and (6) require the evaluation of temperature gradients and the shear stresses at the wall. While there are multiple ways to compute such quantities [19, 32-35] with the finite volume and finite difference discretizations, extended stencils are used to get second order accuracy. This can be done on structured meshes with one-sided discretization stencils, provided that strict orthogonality is maintained near the wall, but the approach is not generalizable to unstructured meshes. In the FE framework the most immediate way would be by a direct differentiation of the shape functions at the wall. For a Newtonian fluid, the tensor of the viscous stresses is written as

$$\boldsymbol{\tau} = \mu\left(\nabla\mathbf{V} + \nabla\mathbf{V}^{\mathbf{T}}\right) - \tfrac{2}{3}\mu\nabla\cdot\mathbf{V} \tag{7}$$

and the normal shear stress vector is

$$\boldsymbol{\tau}_n = \mathbf{n}\cdot\boldsymbol{\tau} = \mu\left(\mathbf{n}\cdot\nabla\mathbf{V} + (\nabla\mathbf{V})\mathbf{n}\right) - \tfrac{2}{3}\mu\mathbf{n}\nabla\cdot\mathbf{V} \tag{8}$$

Lagrangian shape functions, N_j, are used to approximate the velocity throughout each element as a linear combination of the values at the vertices, i.e.

$$\mathbf{V}(t,\mathbf{x}) = \sum_{j=1}^{N_G} N_j(\mathbf{x})\mathbf{V}_j(t)$$

where N_G is the number of nodes in the mesh, N_j are the Lagrange shape functions of the j-th vertex and $\mathbf{V}_j$ is the value of velocity vector at the j-th node. Substituting the polynomial expansion of the velocity into Eq. (8), one obtains

$$\boldsymbol{\tau}_n = \sum_{j=1}^{N} \mathbf{V}_j \cdot \left[\mu(\mathbf{n}\cdot\nabla N_j + \mathbf{n}\nabla N_j) - \tfrac{2}{3}\mu(\nabla N_j\ \mathbf{n})\right] \tag{9}$$

or, by components

$$(\boldsymbol{\tau}_n)^\alpha = \sum_{j=1}^{N} \mathbf{V}_j^\alpha \left[\mu \left(\mathrm{n}^\gamma \frac{\partial N_j}{\partial \mathrm{x}^\gamma} + \mathrm{n}^\alpha \frac{\partial N_j}{\partial \mathrm{x}^\beta} \right) - \frac{2}{3} \mu \mathrm{n}^\beta \frac{\partial N_j}{\partial \mathrm{x}^\alpha} \right]$$

Eq. (9) can be used directly in Eq. (4) to evaluate the slip velocity for rarefied flows. Following the same finite element methodology, the gradient of temperature can be approximated as

$$\nabla T \cdot \mathbf{n} = \sum_{j=1}^{N} T_j (\mathbf{n} \cdot \nabla N_j) \tag{10}$$

and introduced in Eq. (6) to compute the temperature jump at the wall. The classical formulation just presented is only first-order accurate in space for linear finite elements. Higher accuracy can be achieved without widening the computational stencil but necessitates higher order elements where the degrees of freedom must be kept at a moderate level.

A. Consistent Galerkin Finite-Element Method (CGFEM)

In order to avoid resorting to higher order elements, second order accuracy can be achieved by considering, for each component of $\boldsymbol{\tau}_n$, the corresponding momentum equation in its discretized weak-Galerkin form. Consider the conservation of momentum in the *x*-direction for a compressible fluid

$$\frac{\partial \rho u}{\partial t} + \nabla \cdot (\mathbf{F} - \boldsymbol{\tau}_x) = 0 \tag{11}$$

where **F** represents the inviscid flux vector and $\boldsymbol{\tau}_x$ is the stress vector in the *x*-direction. Introducing a set of linear weight functions W_i and integrating by parts, Eq. (11) becomes

$$\int_\Omega W_i \frac{\partial \rho u}{\partial t} - \int_\Omega \nabla W_i \cdot \left(\mathbf{F} - \boldsymbol{\tau}_x \right) + \int_{\partial\Omega} W_i \, \mathbf{n} \cdot \left(\mathbf{F} - \boldsymbol{\tau}_x \right) = 0 \tag{12}$$

At steady state, the *x*-component of the stresses normal to the surface can be written as

$$\int_{\partial\Omega} W_i \, (\mathbf{n} \cdot \boldsymbol{\tau})_x = -\int_\Omega \nabla W_i \cdot \left(\mathbf{F} - \boldsymbol{\tau}_x \right) + \int_{\partial\Omega} W_i \, \mathbf{n}_i \cdot \mathbf{F} \tag{13}$$

Only the first layer of elements near walls needs to be considered and the right-hand-side is constructed during the assembly of the momentum equations. The solution of Eq. (13) yields the nodal values of the normal shear stress tensor projected along the *x*-coordinate. A mass matrix results from the left-hand-side of Eq. (13), and is replaced by

its lumped counterpart. The same approach is applied to the calculation of the wall temperature gradient. The weak-Galerkin form of the energy equation is

$$\int_{\Omega} W_i \frac{\partial \rho e}{\partial t} - \int_{\Omega} \nabla W_i \cdot \left(\rho h \mathbf{V} - \mathbf{V} \cdot \boldsymbol{\tau} - k \nabla T \right) + \int_{\partial\Omega} W_i \, \mathbf{n} \cdot \left(\rho h \mathbf{V} - \mathbf{V} \cdot \boldsymbol{\tau} - k \nabla T \right) = 0 \tag{14}$$

where h is the total enthalpy per unit mass and e is the total energy per unit mass. At steady state, the normal heat flux at the wall is thus

$$-\int_{\partial\Omega} W_i \, \mathbf{n} \cdot k \nabla T = \int_{\partial\Omega} W_i \, \mathbf{q} \cdot \mathbf{n} = \int_{\Omega} \nabla W_i \cdot \left(\rho h \mathbf{V} - \mathbf{V} \cdot \boldsymbol{\tau} - k \nabla T \right) - \int_{\partial\Omega} W_i \, \mathbf{n} \cdot \left(\rho h \mathbf{V} - \mathbf{V} \cdot \boldsymbol{\tau} \right) \tag{15}$$

The same methodology outlined for the normal shear stresses can be used to obtain $k \nabla T \cdot \mathbf{n}$ at surface nodes. Having obtained the values of the normal component of the heat flux and shear stress, equations (4) and (6) can then be enforced as Dirichlet conditions with the following procedure, illustrated in Figure 1.

a. Assembly of the residual and the Jacobian matrix of the Navier-Stokes equations.
b. Imposition of a Dirichlet condition for the temperature and velocity based on their current value using relaxation.
c. Solution of the Newton step and update of the conservative variables, with $\Delta T = 0$ and $\Delta \mathbf{V} = 0$.
d. Computation of the normal shear stress and heat flux via Eq. (13) and (15).
e. Update of the velocity and temperature field at the wall using Eq. (4) and (6), respectively.

The procedure is repeated until convergence.

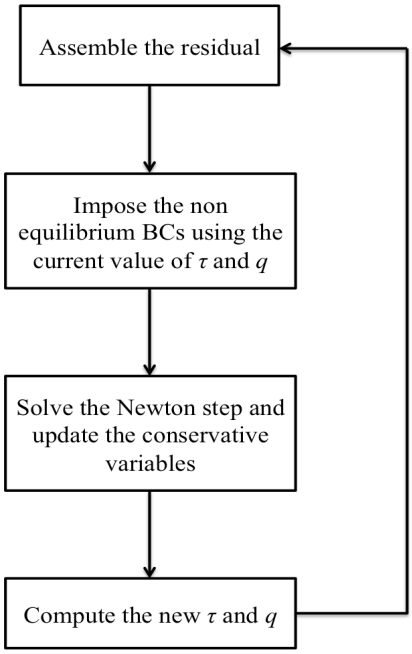

Figure 1. Algorithm for the imposition of the velocity slip and temperature jump using CGFEM.

IV. Numerical Experiments

The purpose of this investigation is to validate the accuracy of the proposed CGFEM formulation of the slip conditions in terms of surface properties, such as heat flux and shear stress at the wall. The wall-related quantities are evaluated in terms of surface friction and surface heating coefficients

$$C_f = \frac{2\tau}{\rho_\infty U_\infty^2} \qquad C_h = \frac{2q}{\rho_\infty U_\infty^3} \tag{16}$$

Several test cases are examined considering simple geometrical configurations as a cylinder and a sphere. These geometries are simple but provide insight on the behavior of the aerodynamic interaction in presence of curved surfaces and are therefore a relevant preliminary test bed for subsequent more complex configurations. First, the two-dimensional Mach 10 flow of Argon past a cylinder is considered, for which reference data is available [1]. The tests are performed for Knudsen numbers ranging from 0.01 to 0.25. Subsequently, the methodology is tested on a Mach 10 flow of Nitrogen past a sphere [29]. The simulations are performed over the same Kn_∞ range, 0.01, 0.05 and 0.25. In all cases, the gas is treated as a single fluid with no chemical activity and thermal equilibrium is assumed among all energy modes such that a single temperature characterizes the flow.

Argon gas flow over a cylinder at Mach 10

The hypersonic laminar flow of Argon around a cylinder section at $M_\infty = 10$ is considered. The temperature of the free stream flow is 200 K and the velocity 2624 m/s. The Knudsen numbers are 0.01, 0.05 and 0.25 corresponding to densities of 2.818×10^{-5}, 5.636×10^{-6} and 1.127×10^{-6} kg/m^3, respectively. Table 1 reports the Knudsen, Reynolds and Mach numbers, for which the simulations have been performed, with the Reynolds number computed using the diameter of the cylinder. Argon has a specific heat ratio $\gamma = 1.67$ and Prandtl number $Pr = 0.667$. The Variable Hard Sphere (VHS) model [36] is adopted for the viscosity, while the thermal conductivity is defined by the Eucken relation as

$$\mu = \mu_0 \left(\frac{T}{T_0} \right)^{\omega} \qquad k = \frac{9\gamma - 5}{4\gamma - 4} R\mu \tag{17}$$

where $\mu_0 = 5.07 \times 10^{-5}$ kg/m s, $T_0 = 1000.0$ K and $\omega = 0.734$, ω is the temperature exponent of the VHS model and R is the specific gas constant of Argon, namely 208.1 J kg/K.

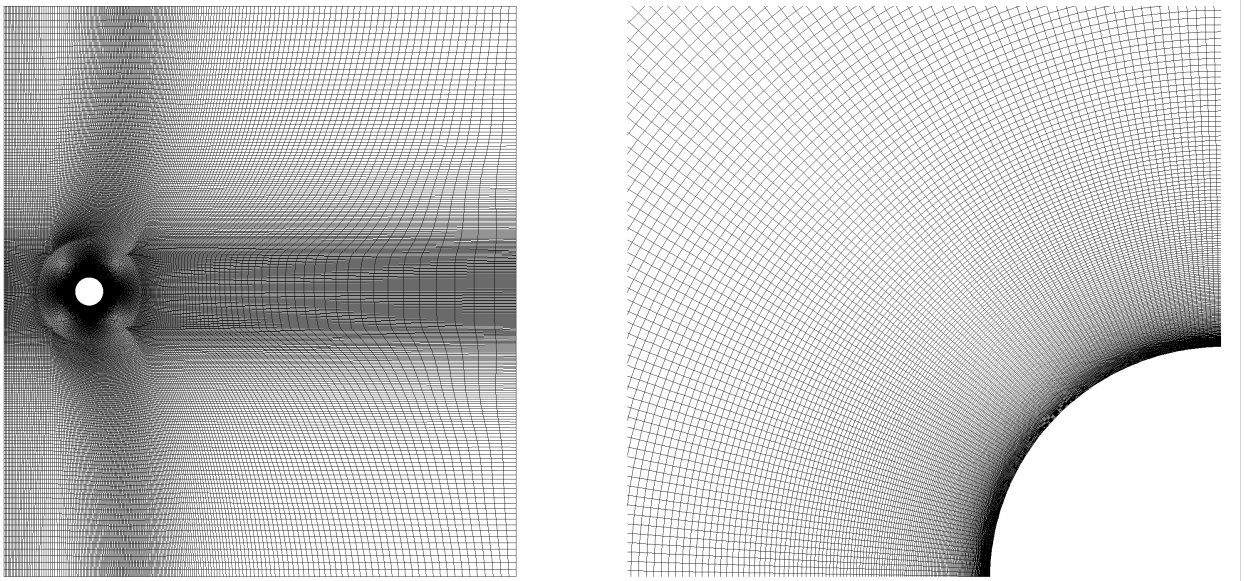

Figure 2. Computational mesh for the flow past a cylinder. Full grid (left), forebody close-up (right).

Kn_∞	Re_∞	M_∞	Regime
0.01	4000	10	Continuum
0.05	800	10	Slip Regime
0.25	160	10	Transitional

Table 1. Values of relevant non-dimensional groups for the simulation of high-speed Argon flow past a cylinder.

Figure 2 shows the computational mesh consisting of 252,600 nodes and 125,600 hexahedra. In order to clearly identify the regions where non-equilibrium is occurring, a continuum breakdown parameter has been adopted [3, 4]. The local Knudsen number can be introduced as

$$\mathrm{Kn}_{\rho} = \lambda \left| \frac{\nabla \rho}{\rho} \right| \tag{18}$$

Figure 3 and 4 show the continuum breakdown on the domain for the cases considered. At Kn = 0.01 and Kn = 0.05, significant non-equilibrium effects are observed in the shock, in the boundary layer and in the wake regions. At Kn = 0.25 the non-equilibrium effects are generalized through the domain and dominate the gas behavior. Figure 5 presents the continuum breakdown at the wall of the body, where important non-equilibrium effects can be observed in the rear part of the cylinder for Kn 0.01, 0.05 and 0.25. An angle of 0 corresponds to the stagnation point and an angle of 180 is located at the rear stagnation point. Note that as the Knudsen Number increases, the non-equilibrium effects do not just occupy a greater region of the domain, but their level increases as well; reaching as high as 100, well into the free-molecular flow regime.

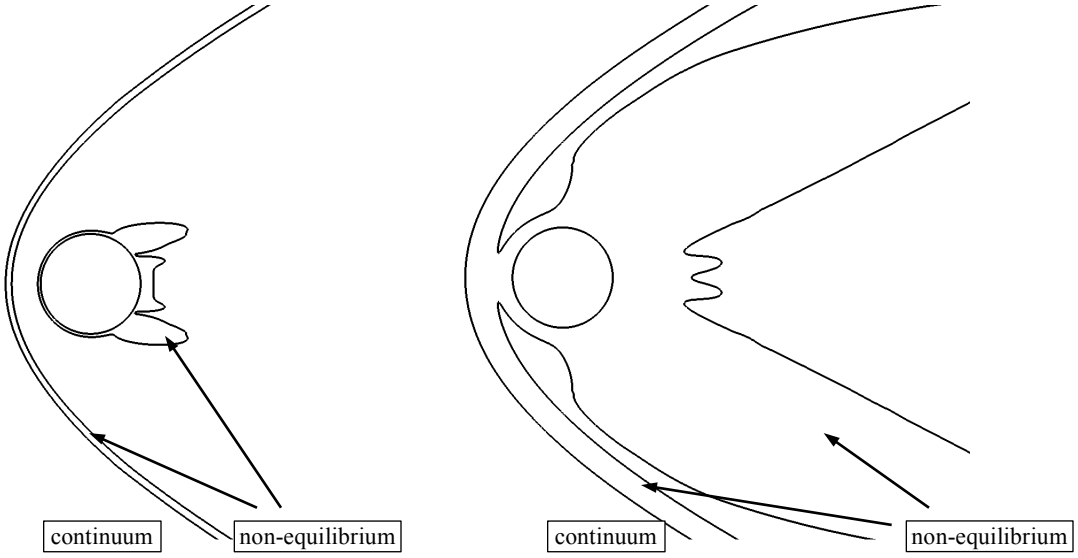

Figure 3. Continuum-breakdown at Kn = 0.01 (left), at Kn = 0.05 (right).

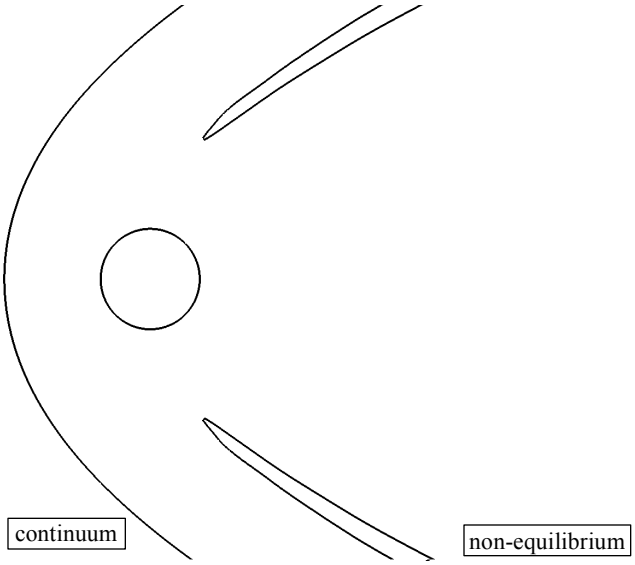

Figure 4. Continuum-breakdown at Kn = 0.25.

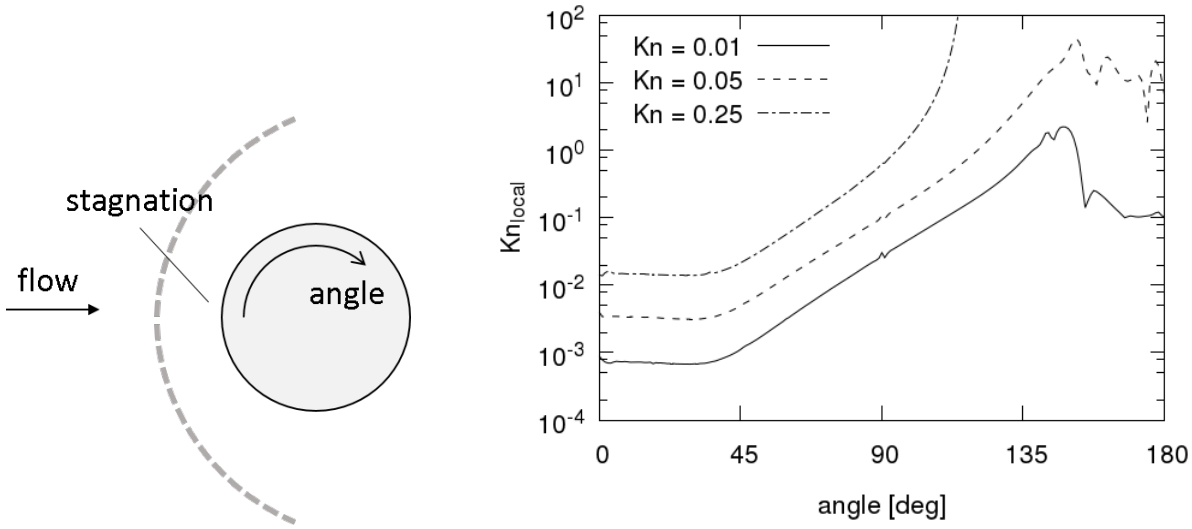

Figure 5. Continuum-breakdown at the wall at Kn = 0.01, 0.05 and 0.25. The stagnation point is at 0 deg.

A. Kn = 0.01

A free-stream Knudsen number of 0.01 typically marks the end of the continuum regime and the beginning of the slip regime, where discrepancies between CFD simulations and DSMC begin to appear but are still moderate. DSMC results from [1] are used as reference data to verify the accuracy of the approach.

Figure 6 compares the surface heating coefficient and surface friction coefficient between three different solvers: the proposed method, referred to as High Altitude-Low Orbit (HALO3D), the finite volume CFD solver LeMANS [1] and the DSMC solver MONACO [1]. Also, the solution with non-equilibrium boundary conditions is compared

against the one using no-slip conditions. The curves of the surface coefficients shown in figure 6 indicate a substantial agreement. The peak heating and friction are predicted well by HALO3D. In addition, the non-equilibrium boundary conditions improve the surface heating results, especially in the rear part of the cylinder. The same can be observed for the surface friction coefficient. The slip conditions reasonably improve the agreement with the DSMC solution.

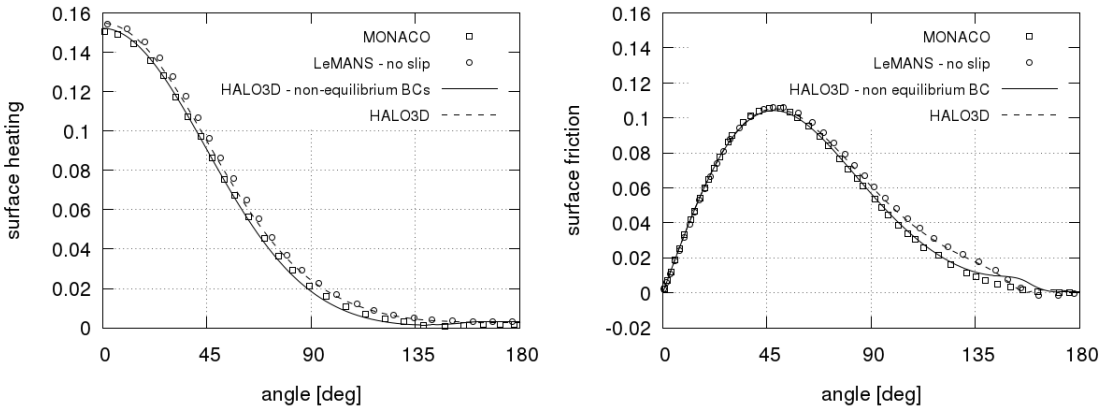

Figure 6. Surface heating coefficient (left) and surface friction coefficient (right), at Kn = 0.01.

B. Kn = 0.05

At a Knudsen number of 0.05, the flow is considered to be in the slip regime and the slip conditions should provide a significant improvement over the nonslip boundary conditions for the surface properties. Indeed, compared to Kn = 0.01, at Kn = 0.05 figure 3 shows larger regions of continuum breakdown both in the shock and in the wake region.

In figure 7 (left), the surface heating coefficient agrees well with the DSMC solution even in a more rarefied regime. The CGFEM approach agrees particularly well with the DSMC simulation in the wake region. The present simulations use a standard, calorically- perfect model for Argon, which could explain the slight overprediction of the heat flux at the stagnation point. As shown in figure 7 (right), the surface friction coefficients using the non-equilibrium boundary conditions show some difference with the one obtained with DSMC. The peak magnitude is not perfectly captured. This could be explained in terms of the current implementation not accounting for non-equilibrium mechanisms inside the domain that can influence the dynamics of the fluid approaching the wall. As shown by comparison with LeMANS and HALO3D, the use of slip conditions allows for considerable improvement with respect to DSMC.

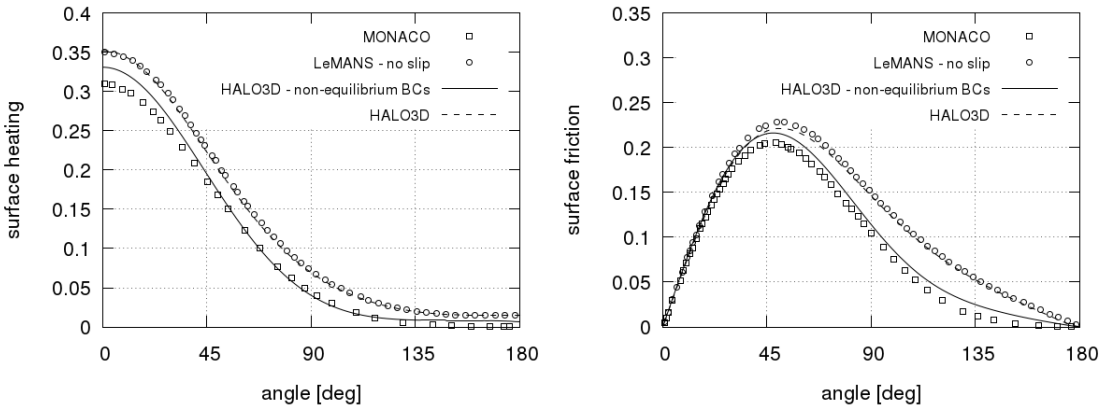

Figure 7. Surface heating coefficient (left) and surface friction coefficient (right) at Kn = 0.05.

C. Kn = 0.25

At a Knudsen number of 0.25, the flow is in non-equilibrium near the cylinder surface. As shown in figure 4, the continuum breakdown region extends completely behind the shock region, and the shock itself moves further away from the cylinder. Therefore, slip conditions are of paramount importance to model the gas behavior for such a high degree of rarefaction.

As shown in figure 8 (left) the surface heating coefficient predicted by HALO3D does not compare well with the DSMC simulation, despite the improvement with respect to the other continuum-based methods. The same can be said for the surface friction coefficient, shown in figure 8 (right). In the transition regime, non-equilibrium boundary conditions are not enough to account for the level of rarefaction, as can be seen from these results.

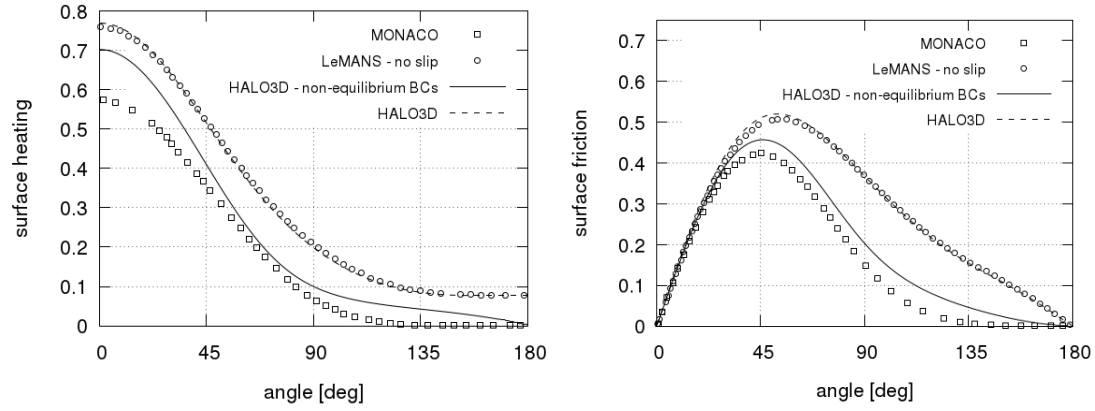

Figure 8. Surface heating coefficient (left) and surface friction coefficient (right) at Kn = 0.25.

Nitrogen gas flow over a sphere at Mach 10

The mesh for this case contains 5,766,176 elements and 2,705,983 nodes (figure 9). The flow conditions are summarized in tables table 2 and table 3. Nitrogen has a specific heat ratio $\gamma = 1.4$, Prandtl number Pr= 0.7368 and gas constant R = 296.8 J kg/K. The VHS model [36] of Eq. (17) is used with $\mu_0=1.67 \times 10^{-5}$ kg/m s, $T_0 = 273.0$ K and $\omega=0.75$. R in this case, is the specific gas constant of Nitrogen. The results are shown at the symmetry plane of the sphere.

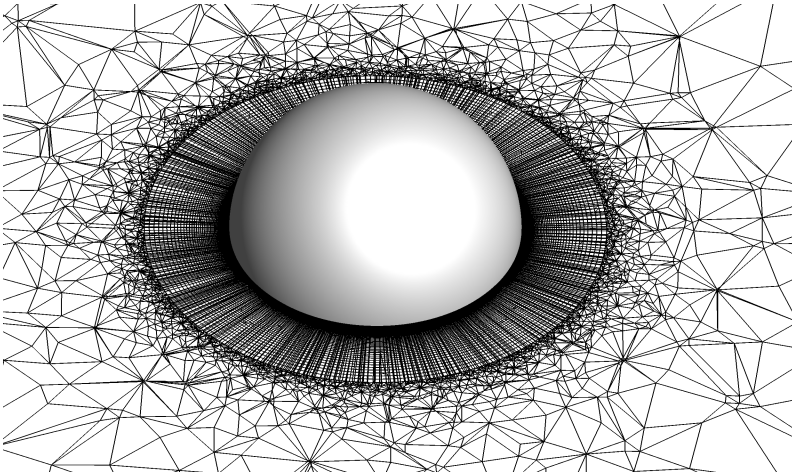

Figure 9. Computational mesh for flow over a sphere.

Velocity	2884 m/s
Mach number	10
Free stream temperature	200 K

Table 2. Flow properties for the flow of Nitrogen over a sphere at Mach 10.

ρ_∞	Pressure	Kn_∞	Re_∞
1.975 x 10^{-5} kg/m^3	1.17 Pa	0.01	1280
3.949.975 x 10^{-6} kg/m3	0.23 Pa	0.05	256
7.899 x 10^{-7} kg/m^3	0.047 Pa	0.25	51.2

Table 3. Simulated regime for the flow of Nitrogen over a sphere.

A. Kn = 0.01

As shown in figure 10, at Kn = 0.01, non-equilibrium effects are present in the shock, boundary layer and wake regions. Although this global Knudsen number is not commonly associated with a fully-rarefied flow, local breakdown regions appear where the flow behaves in a rarefied manner and thus requires a suitable treatment of the near-wall region.

Figure 11 shows the comparison of the surface heating and surface friction coefficients with the solutions obtained with LeMANS, MONACO and HALO3D. The peak heating (left) is over-predicted in the solution with

slip conditions while slight improvements are observed in the wake region. Note however, that DSMC includes variable vibrational and rotational energy exchange models, whereas HALO3D currently does not. For the surface friction (right), the temperature jump and velocity slip fairly improve the agreement with DSMC, particularly in the wake region.

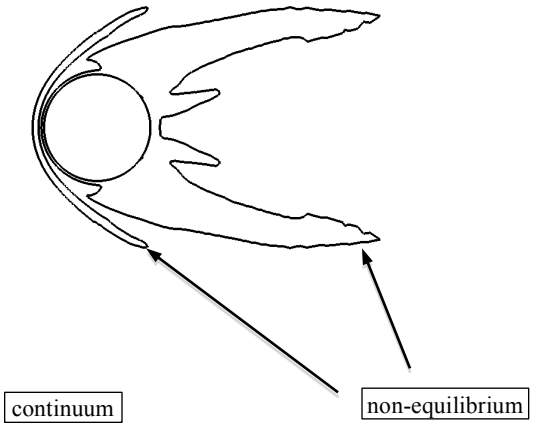

Figure 10. Continuum-breakdown at Kn = 0.01.

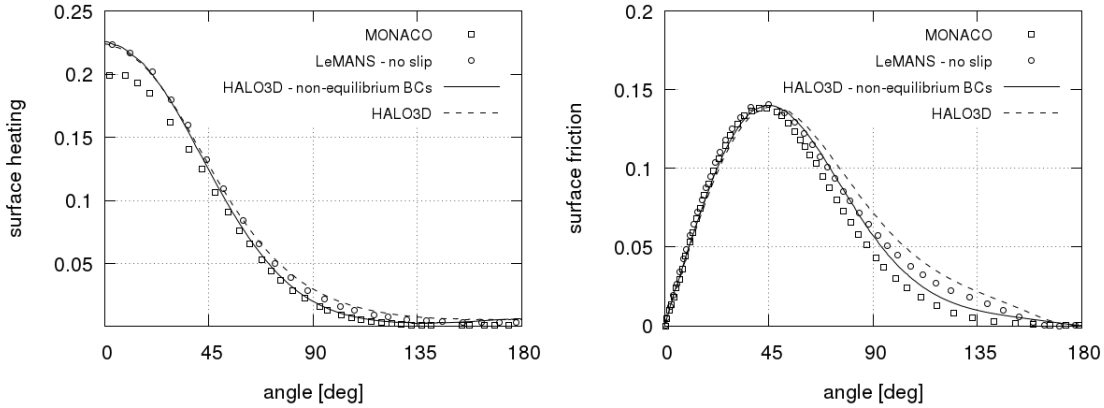

Figure 11. Surface heating coefficient (left) and surface friction coefficient (right) at Kn = 0.01 across the center of the sphere.

B. Kn = 0.05

At the global Kudsen number of 0.05 the non-equilibrium regions become more important, as shown in figure 12. The shock stand-off distance has increased.

Figure 13 shows that the surface heating coefficient is over-predicted by HALO3D at the stagnation point. The surface friction coefficient does not match well with the DSMC simulation shown in figure 13 (left). The peak friction coefficient location has moved slightly further on the sphere with the slip and non-slip conditions. However, the agreement with DSMC for the wake region improves with the non-equilibrium boundary conditions. Overall, the proposed slip conditions improve the prediction of shear stress and heat flux, particularly in the wake region.

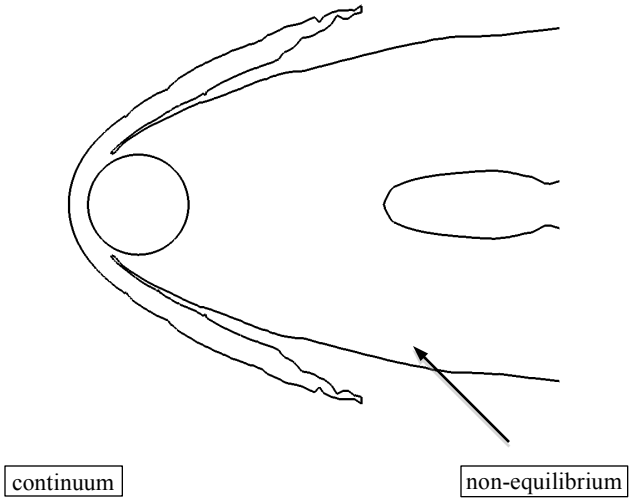

Figure 12. Continuum-breakdown at Kn = 0.05.

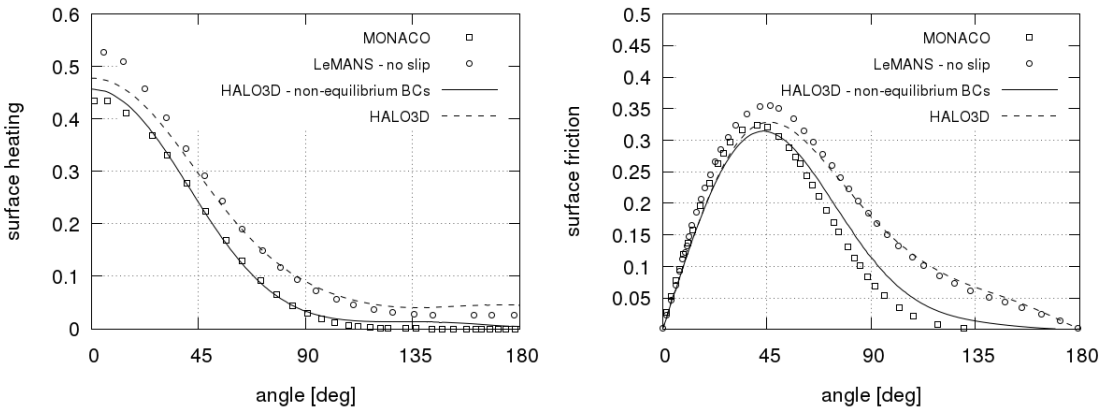

Figure 13. Surface heating coefficient (left) and surface friction (right) coefficient at Kn = 0.05 across the center of the sphere.

C. Kn = 0.25

At Kn = 0.25, the treatment of the continuum breakdown effects is critical. Figure 14 shows the gradient-length-local Knudsen number where the flow is almost entirely in non-equilibrium.

Figure 15 presents the surface heating and friction coefficients where the various solvers are no longer in agreement. HALO3D with slip condition overestimate both surface properties with respect to DSMC near the fore body of the sphere for the surface heating coefficient and near the wake region for the surface friction coefficient. The heat flux (left) and shear stress (right) show large difference between the DSMC solver and the FEM CFD code. At this Knudsen number, the slip conditions alone are not sufficient to address the continuum breakdown. More sophisticated strategies are required. Nonetheless, the slip conditions allow for an improvement in the heat flux prediction. The same can be said for the surface shear stress, where, even though the differences between DSMC and HALO3D are still important, the differences are minimized with the slip conditions.

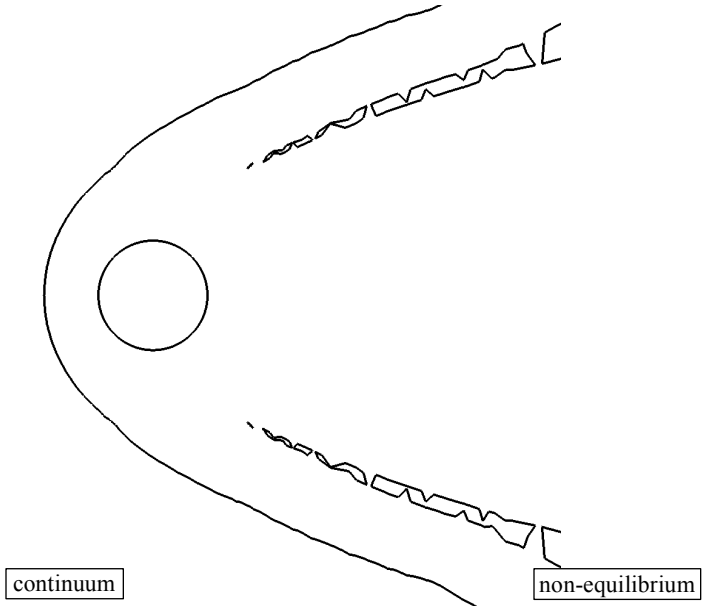

Figure 14. Continuum-breakdown at Kn = 0.25.

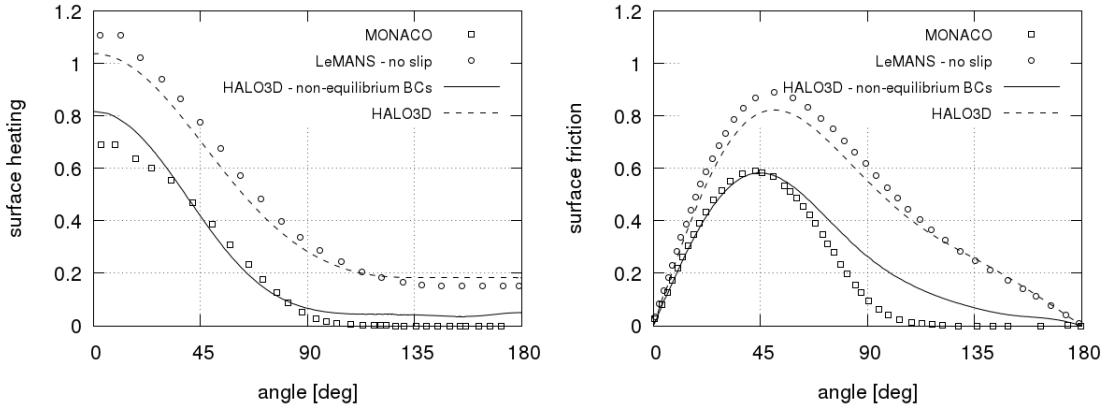

Figure 15. Surface heating (left) and surface friction (right) coefficient at Kn = 0.25 across the center of the sphere.

V. Order of accuracy

The computational cost, in terms of time and computational resources, to obtain adequate accuracy for engineering purpose often constitutes a major constraint on the application of CFD to aerothermodynamics design. One solution is to use higher accuracy methods to decrease the computational footprint necessary to achieve an acceptable error level by alleviating the grid spacing requirements. In this section, the spatial order of accuracy of the proposed methodology and the direct approach is evaluated for the heat flux and the shear stress. The analysis is performed through a sequential grid refinement analysis using nested uniformly-refined meshes, for the flow of Argon over a cylinder at Kn = 0.01; the simulation described in section IV

In the context of Finite Elements, the L_2 norm for the heat flux is computed as:

$$L_2(\partial\Omega) = \left[\frac{\int_{\partial\Omega} \left(q - q^{exact} \right)^2 dA}{\int_{\partial\Omega} dA} \right]^{1/2} = \left[\frac{\sum_{i=1}^{N} \left(q_i - q_i^{exact} \right)^2 \left| A_i \right|}{\sum_{i=1}^{N} \left| A_i \right|} \right]^{1/2} \tag{19}$$

where the norm is integrated over the area since the heat flux is defined strictly on the surface. A similar formulation is used to compute the L_2 norm for the shear stress. The error is computed using the reference solution obtained with the mesh with the highest resolution. Table 4 presents the computational details of the four successively refined grids.

Grid	Grid spacing: h	Elements	Nodes	Surface nodes
1	8	4,000	8,160	80
2	4	16,000	32,320	160
3	2	64,000	128,640	320
4	1	256,000	513,280	640

Table 4. Details of the meshes used for the grid refinement analysis.

Figure 16 shows the results of the convergence study for the heat flux. Using nonlinear least-squares algorithm for the fitting model, an order of accuracy of 0.95 for the direct approach is achieved, and an order of accuracy of 1.77 for the CGFEM. The expected order of accuracy is achieved for both schemes, with the CGFEM showing improved performance over the direct approach. Figure 17 compares the surface heating coefficient obtained by both approaches on the four different meshes. The advantage of using a higher order scheme is readily apparent: The solution of the CGFEM on the coarsest grid is more accurate than the solution of the direct approach on a mesh 8

times denser. Figure 18 and figure 19 present the order of accuracy for the x-component and y-component of shear stress, respectively, while figure 20 shows the resulting surface friction coefficient for both methodologies. The slope obtained from the linear fit of the results yields an order of accuracy of 1.62 for the x-component and 1.63 for the y-component of shear stress for the CGFEM, demonstrating that the accuracy of the methodology is not overly contaminated by the presence of the shock.

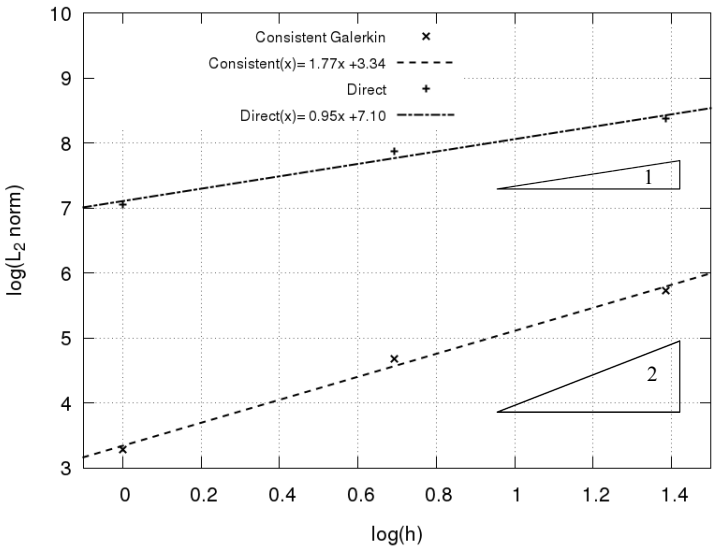

Figure 16. Flow of Argon over a cylinder at Kn = 0.01: order of accuracy of the heat flux.

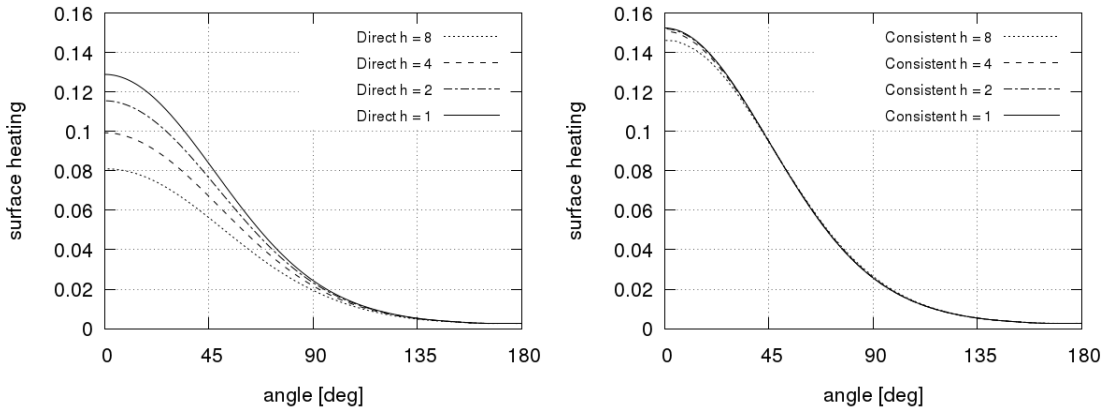

Figure 17. Direct approach for the surface heating coefficient (left) and CGFEM for the surface heating coefficient (right) on uniformly-refined meshes.

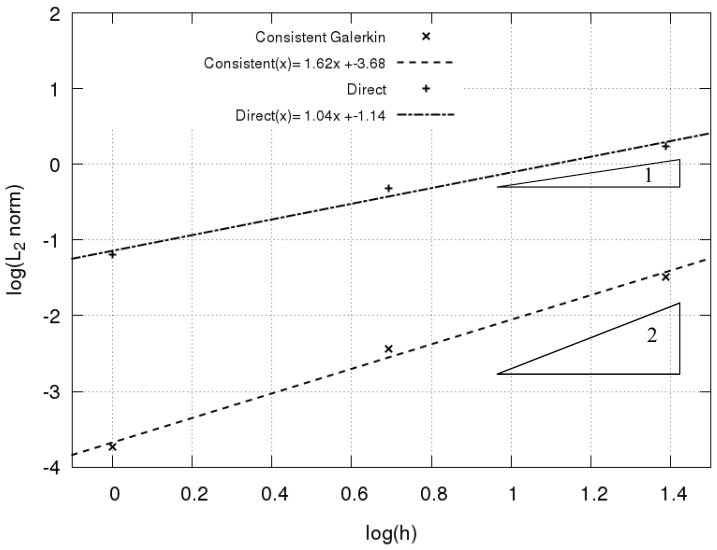

Figure 18. Flow of Argon over a cylinder at Kn = 0.01: order of accuracy of the x-component of shear stress.

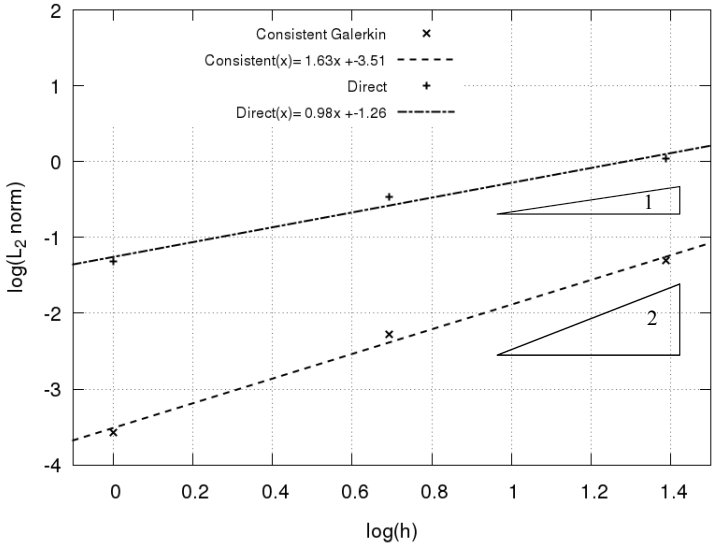

Figure 19. Flow of Argon over a cylinder at Kn = 0.01: order of accuracy of the y-component of shear stress.

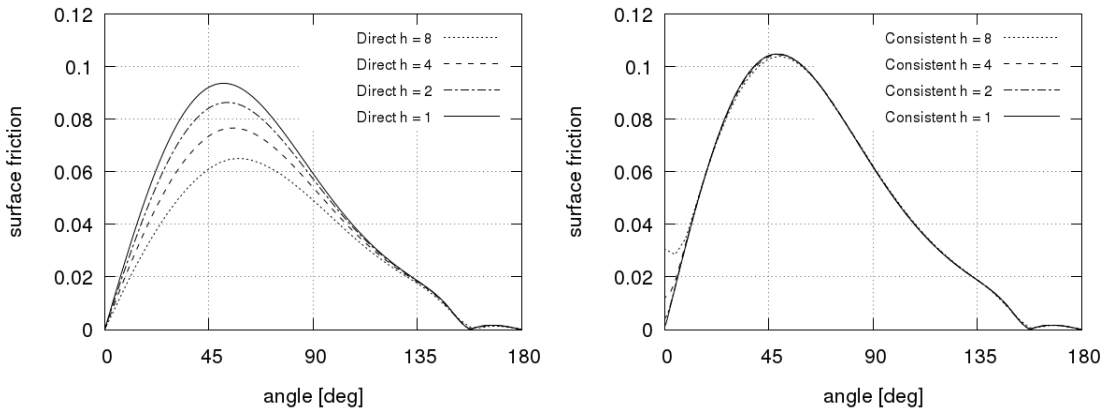

Figure 20. Direct approach for the surface friction coefficient (left) and CGFEM for the surface friction coefficient (right) on uniformly-refined meshes.

VI. Conclusions

A Consistent Galerkin Finite Element Method is proposed to discretize existing boundary condition models for non-equilibrium regimes with second order spatial accuracy. The method relies on the re-evaluation of both the momentum and energy equations using previously computed integrals. The order of convergence of the methodology is confirmed by a grid-refinement analysis where the robustness of the methodology is demonstrated in the presence of shocks. Tests performed on a cylinder and a sphere at very high speeds in regimes ranging from continuum to transitional show the advantages of the proposed methodology, as well as some its remaining limitations and issues. The results show that at large Knudsen number, the difference in aerothermodynamics properties between CFD and DSMC are significant, highlighting the necessity to have non-equilibrium boundary conditions to address the breakdown of the assumption of continuity in the Navier-Stokes equations. For all simulations, however, agreement with DSMC improved with the more accurate slip conditions, particularly in the wake of the two geometries. Nevertheless, from the results, it is also clear that boundary conditions by themselves are insufficient to model accurately high-Mach / rarefied regimes. Treatment of the non-equilibrium effects inside the domain is also necessary, using methods that account for thermal and chemical non-equilibrium. This calls for other approaches that allow the introduction of macroscopic methods based on kinetic theory of gases within the Finite Element framework to extend the applicability of the macroscopic approach to values of the Knudsen number approaching unity.

Acknowledgments

The authors would like to thank the NSERC-Lockheed Martin-Bell Helicopter Industrial Research Chair whose generous financial support permitted this work. We are also grateful to Compute Canada and CLUMEQ for the access to their computing resources that facilitated this work.

References

[1] Lofthouse, A.J., "Non-equilibrium Hypersonic Aerothermodynamics Using the Direct Simulation Monte Carlo and Navier-Stokes Models" 2008.

[2] Anderson, J.D., "Hypersonic and High-Temperature Gas Dynamics" American Institute of Aeronautics and Astronautics, 1989.

[3] Boyd, I.D., "Predicting Breakdown of the Continuum Equations Under Rarefied Flow Conditions" *AIP Conference Proceedings,* Vol. 663, No. 1, 2003, pp. 899-906.

[4] Lofthouse, A.J., Scalabrin, L.C., Boyd, I.D., "Velocity Slip and Temperature Jump in Hypersonic Aerothermodynamics" *Journal of Thermophysics and Heat Transfer,* Vol. 22, No. 1, 2008, pp. 38-49.

[5] Wang, W., Boyd, I.D., "Predicting continuum breakdown in hypersonic viscous flows" *Physics of Fluids,* Vol. 15, No. 1, 2003, pp. 91-100.

[6] Wang, W., Sun, Q., Boyd, I.D., "Towards Development of a Hybrid DSMC-CFD Method for Simulating Hypersonic Interacting Flows" *8th AIAA/ASME Joint Thermophysics and Heat Transfer Conference,* American Institute of Aeronautics and Astronautics, 2002.

[7] Wang, W., Boyd, I.D., "Hybrid DSMC-CFD Simulations of Hypersonic Flow over Sharp and Blunted Bodies" *36th AIAA Thermophysics Conference,* American Institute of Aeronautics and Astronautics, 2003.

[8] Carlson, H., Roveda, R., Boyd, I.D., "A Hybrid CFD-DSMC Method of Modeling Continuum-Rarefied Flows" *42nd AIAA Aerospace Sciences Meeting and Exhibit,* American Institute of Aeronautics and Astronautics, 2004.

[9] Burt, J.M., Boyd, I.D., "A Hybrid Particle Approach for Continuum and Rarefied Flow Simulation" *Journal of Computational Physics,* Vol. 228, No. 2, 2009, pp. 460-475.

[10] Schwartzentruber, T., Boyd, I.D., "Detailed Analysis of a Hybrid CFD-DSMC Method for Hypersonic Non-Equilibrium Flows" *38th AIAA Thermophysics Conference,* American Institute of Aeronautics and Astronautics, 2005.

[11] Maxwell, J.C., "On Stresses in Rarified Gases Arising from Inequalities of Temperature" *Philosophical Transactions of the Royal Society of London,* Vol. 170, 1879, pp. 231-256.

[12] Gökçen, T., MacCormack, R.W., "Nonequilibrium Effects for Hypersonic Transitional Flows Using Continuum Approach" *27th Aerospace Sciences Meeting,* American Institute of Aeronautics and Astronautics, 1989.

[13] Fichman, M., Hetsroni, G., "Viscosity and Slip Velocity in Gas Flow in Microchannels" *Physics of Fluids,* Vol. 17, No. 12, 2005.

[14] Arkilic, E.B., Breuer, K.S., Schmidt, M.A., "Mass Flow and Tangential Momentum Accommodation in Silicon Micromachined Channels" *Journal of Fluid Mechanics,* Vol. 437, 2001, pp. 29-43.

[15] Greenshields, C.J., Reese, J.M., "Rarefied Hypersonic Flow Simulations Using the Navier–Stokes Equations with Non-equilibrium Boundary Conditions" *Progress in Aerospace Sciences,* Vol. 52, 2012, pp. 80-87.

[16] Lockerby, D.A., Reese, J.M., Emerson, D.R., "Velocity Boundary Condition at Solid Walls in Rarefied Gas Calculations" *Physical Review,* Vol. 70, No. 1, 2004.

[17] Barber, R.W., Sun, Y., Gu, X.J., "Isothermal Slip Flow Over Curved Surfaces" *Physics of Fluids,* Vol. 76, No. 1, 2004, pp. 73-81.

[18] Gresho, P.M., "Some Current CFD Issues Relevant to the Incompressible Navier-Stokes Equations" *Computer Methods in Applied Mechanics and Engineering,* Vol. 87, No. 2, 1991, pp. 201-252.

[19] Gresho, P.M., Lee, R.L., Sani, R.L., "The Consistent Galerkin FEM for Computing Derived Boundary Quantities in Thermal and or Fluids Problems" *International Journal for Numerical Methods in Fluids,* Vol. 7, No. 4, 1987, pp. 371-394.

[20] Li, Q., Fu, S., Xu, K., "Application of Gas-Kinetic Scheme with Kinetic Boundary Conditions in Hypersonic Flow" *AIAA Journal,* Vol. 43, No. 10, 2005, pp. 2170-2176.

[21] Le, N.T.P., White, C., Reese, J.M., "Langmuir–Maxwell and Langmuir–Smoluchowski Boundary Conditions for Thermal Gas Flow Simulations in Hypersonic Aerodynamics" *International Journal of Heat and Mass Transfer,* Vol. 55, No. 19–20, 2012, pp. 5032-5043.

[22] Kim, S.H., Pitsch, H., Boyd, I.D., "Slip Velocity and Knudsen Layer in the Lattice Boltzmann Method for Microscale Flows" *Physical Review,* Vol. 77, No. 2, 2008.

[23] Sharipov, F., Kalempa, D., "Velocity Slip and Temperature Jump Coefficients for Gaseous Mixtures. II. Thermal Slip Coefficient" *Physics of Fluids,* Vol. 16, No. 3, 2004, pp. 759-764.

[24] Lockerby, D.A., Reese, J.M., Gallis, M.A., "Capturing the Knudsen Layer in Continuum-Fluid Models of Nonequilibrium Gas Flows" *AIAA Journal,* Vol. 43, No. 6, 2005, pp. 1391-1393.

[25] Millikan, R.A., "Coefficients of Slip in Gases and the Law of Reflection of Molecules from the Surfaces of Solids and Liquids" *Physical Review,* Vol. 21, No. 3, 1923, pp. 217-238.

[26] Sharipov, F., Seleznev, V., "Data on Internal Rarefied Gas Flows" *Journal of Physical and Chemical Reference Data,* Vol. 27, No. 3, 1998, pp. 657-706.

[27] Emerson, D.R., Gu, X., Stefanov, S.K., "Nonplanar Oscillatory Shear Flow: From the Continuum to the Free-Molecular Regime" *Physics of Fluids,* Vol. 19, No. 10, 2007.

[28] Albertoni, S., Cercignani, C., Gotusso, L., "Numerical Evaluation of the Slip Coefficient" *Physics of Fluids,* Vol. 6, No. 7, 1963, pp. 993-996.

[29] Holman, T.D., "Numerical Investigation of the Effects of Continuum Breakdown on Hypersonic Vehicle Surface Properties" 2010.

[30] Smoluchowski, V.S., "Ueber Wärmeleitung in Verdünnten Gasen" *Annalen Der Physik,* Vol. 300, No. 1, 1898, pp. 101-130.

[31] Karniadakis, G., Beskok, A., Aluru, N., "Microflows and Nanoflows: Fundamentals and Simulation" Springer, 2005.

[32] Fossati, M., Guardone, A., Vigevano, L., "Kinetic Node-Pair Formulation for Two-Dimensional Flows from Continuum to Transitional Regime" *AIAA Journal,* Vol. 51, No. 4, 2013, pp. 784-796.

[33] Schwartzentruber, T., Boyd, I.D., "Investigation of Continuum Breakdown in Hypersonic Flows Using a Hybrid DSMC-NS Algorithm" *40th Thermophysics Conference,* American Institute of Aeronautics and Astronautics, 2008.

[34] Oliver, T.A., "A High-Order, Adaptive, Discontinuous Galerkin Finite Element Method for the Reynolds-Averaged Navier-Stokes Equations" 2008.

[35] Fidkowski, K.J., "A High-Order Discontinuous Galerkin Multigrid Solver for Aerodynamic Applications" 2004.

[36] Bird, G.A., "Molecular Gas Dynamics and the Direct Simulation of Gas Flows" Oxford University Press, 1994.